AJP

ISSN : 0971 - 3093

Vol 28, No 3, February 2019

ASIAN JOURNAL OF PHYSICS

An International Peer Reviewed Research Journal

Advisory Editors : W. Kiefer & FTS Yu

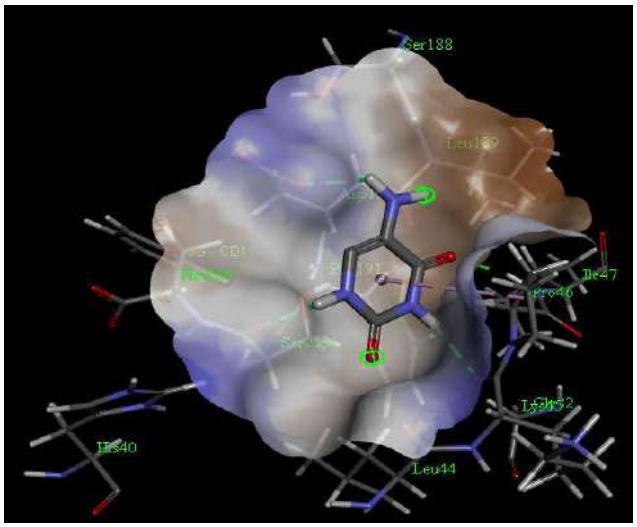

The 3D representation of docked ligand (5-AU) at the binding site (hydrophobic pocket) of the targeted protein hCA I

ap

ANITA PUBLICATIONS

FF-43, 1st Floor, Mangal Bazar, Laxmi Nagar, Delhi-110 092, India

B O : 2, Pasha Court, Williamsville, New York-14221-1776, USA

ap

Asian Journal of Physics
Vol. 28, No 3 (2019) 159-175
Available on: www.asianjournalofphysics.in

Quantum chemical and molecular docking studies on biomolecule 5-Aminouracil

R Premkumar[1], S Christopher Jeyaseelan[1], W Kiefer[2], M A Palafox [3], A Milton Franklin Benial[1] and V K Rastogi[4]

[1]*PG and Research Department of Physics, N M S S V N College, Madurai-625 019, Tamil Nadu, India.*
[2] *Institute for Physical and Theoretical Chemistry, University of Würzburg, Germany, and Eisingen Laboratory for Applied Raman Spectroscopy, Eisingen, Germany*
[3]*Departamento de Química-Física I, Facultad de Ciencias Químicas, Universidad Complutense, Ciudad Universitaria, Madrid-28040, Spain.*
[4]*Indian Spectroscopy Society, KC 68/1, Old Kavinagar, Ghaziabad-201 002, India.*

The quantum chemical studies of 5-aminouracil (5-AU) molecule were performed by density functional theory calculations using Gaussian 09 program. In addition, molecular docking analysis of the molecule was carried out to evaluate the inhibitory nature of the molecule. In the present study, the molecular structure of the molecule was optimized by DFT/B3LYP method with 6-311++G (d,p) basis set using Gaussian 09 program. The frontier molecular orbitals and their related molecular properties were computed, which reveal that the molecule has higher chemical reactivity and stability. The density of states spectrum of the molecule was simulated to validate the FMOs results. The solvent effects on UV-Visible absorption spectra of the molecule were studied. The bathochromic shift and hyperchromic shift were observed going from the gas phase to solvent in the UV-Vis spectra. The first order hyperpolarizability of molecule was calculated, which is 4.51 times greater than the value of urea. The molecular electrostatic potential surface and local reactivity descriptors analysis predict the possible reactive sites of the molecule. The natural bond orbital analysis confirms the bioactive nature of the molecule. The molecular docking analysis shows that the good inhibitory nature of the 5-AU molecule against the human carbonic anhydrase I (hCA I) enzyme, which causes the glaucoma. These results pave the way for developing the effective therapies in the treatment of glaucoma.

Keywords: 5-Aminouracil, DFT, FMOs, UV-Visible, NLO, MEP, Fukui functions, Molecular Docking; Glaucoma.

1 Introduction

The uracil and its derivatives are nitrogen containing heterocyclic compounds have received considerable attention among all series of derivatives of nucleic pyrimidine bases due to their paramount applications in pharmaceutical including anti-microbial, acaricidal, analgesic, anti-inflammatory and anticancer activities [1-4]. The 5-substituted uracils exhibit significant pharmacological activity and they can be used as antitumour, antibacterial and antiviral drugs [5]. Among the 5-subsituted uracil derivatives, 5-aminouracil (5-AU) plays special attention due to its broad range of medicinal applications [6]. 5-AU is a pyrimidine nucleobase analogue of thymine in which the methyl group is replaced by amino group, adding therefore new hydrogen bonding sites. 5-AU has been used as a starting material for the synthesis of other pyrimidines [7,8] or transition metal complexes [9]. In General, uracil helps enzymes to carry out different reactions in cells of human body and also useful in the drug industry with delivering drugs throughout the body. Recently, the bioactive uracil derivatives have been reported as potent inhibitor against human carbonic anhydrase (hCA) that might be useful in medical applications [10].

Corresponding author :
e-mail: miltonfranklin@yahoo.com (A Milton Franklin Benial); v_krastogi@rediffmail.com (V K Rastogi)

The hCA is a ubiquitous family of zinc-containing enzymes, which participate in the maintenance of pH homeostasis in the human body and catalyzing the reversible hydration of carbon dioxide to yield bicarbonate and protons [11]. The members of hCA are involved in diverse physiological functions including pH regulation, ion transport, bone resorption and secretion of gastric, cerebrospinal fluid and pancreatic juices. The most important function of hCA is related to the respiration and transport of CO_2/bicarbonate in various metabolizing tissues. Many hCA isozymes involved in these processes are important therapeutic targets of various disorders such as edema, glaucoma, obesity, cancer, epilepsy and osteoporosis [12,13]. In general, the members of hCA including hCA I, hCA II, hCA IX and hCA XII are reported as important targets for the drug designing [13-16].

Human carbonic anhydrase I (hCA I) is the most abundant non-hemoglobin protein in the red blood cells. hCA I might be an essential component of human red blood cells. hCA I is the most abundant protein (after hemoglobin) in human erythrocytes. hCA I is involved in functions such as antireflux defence, gas exchange and ion transport. hCA I may play a role of an indicator to differentiate autoimmune hemolytic anaemia from other types of anaemia. Glaucoma is a chronic, degenerative eye disease, characterised by high intraocular pressure (IOP) that causes irreversible damage to the optic nerve head, resulting in the progressive loss of visual function and eventually blindness. Thus, the hCA I enzyme is identified as potent target for treatment of glaucoma [13].

Human carbonic anhydrase II (hCA II) is present in almost every tissue and organ of our human body, including osteoclasts in bone, choroid plexus epithelia, retinal muller cells, hepatocytes, kidney, oligodendrocytes in brain, salivary glands, erythrocytes and platelets. The major role of hCA II is controlling the pH level in cells by keeping the adequate balance between carbon dioxide and bicarbonate. hCA II triggers the CO_2 exchange in the erythrocytes, lungs and renal proximal tubules [14]. The hCA II is abundant in the bone, which is present in osteoclasts at concentrations of the same order of magnitude as those present in the kidneys. Its role there is to provide hydrogen ions, formed from the hydration of CO_2, to an ATP dependent proton pump, which uses them in the mobilization of calcium from the bone. The defects in the hCA II enzyme produce the autosomal recessive disorder such as osteopetrosis, renal tubular acidosis, and cerebral calcification. Thus, the hCA II enzyme is identified as potent target for treatment of marble brain disease.

Human carbonic anhydrase IX (hCA IX) is predominantly found in tumor cells and shows a restricted expression in normal tissues. A key feature of many tumours is hypoxia. Tumour hypoxia appears to be strongly associated with tumour propagation, malignant progression, and resistance to chemotherapy. The expression of hCA IX is strongly upregulated in hypoxia. hCA IX expression is strongly increased in many types of tumours, such as ependymomas, mesotheliomas, follicular carcinomas, carcinomas of the bladder, uterine cervix, nasopharyngeal carcinoma, breast, oesophagus, lungs, brain, squamous cell carcinomas, and kidney tumours [15]. Therefore, it has been considered that the hCA IX inhibitors are crucial molecules for the synthesis of new-generation anticancer drugs.

Human carbonic anhydrase XII (hCA XII) has been detected in the human gut, including all segments of the large intestine. hCA XII regulates pH and CO_2 homeostasis in different tissues [16]. hCA XII is a membrane-associated enzyme, have been characterized as tumour markers in human cancers. hCA XII expression in breast tumour is indicative of lower grade disease, lower relapse rates, and better overall patient survival. Mutation in hCA XII has also been associated with the cystic fibrosis-like syndrome, including hyponatremia.

Computational tools such as density functional theory (DFT) calculations and molecular docking studies have been proven to be efficient and inexpensive approaches for understanding various fundamental properties of biological molecules and drugs [17, 18]. DFT calculations provide significant information about the stable molecular geometry, vibrational frequencies, charge transfer stabilization interaction, reactive

nature and possible local reactive sites of a molecular system. The local reactivity descriptors pave the way for understanding the interaction between biologically privileged molecular systems, which leads to the search of new pharmaceutical compounds and effective drug designing [19]. The molecular docking study is a powerful computational tool in predicting the binding mode and binding affinity of a ligand with the proteins, which is an effective tool in modern structure-based drug designing [20]. Considering these aspects, a combination of DFT quantum chemical calculations and molecular docking analysis of the 5-aminouracil (5-AU) molecule were performed, which will be useful in the future *in-vivo* studies of this molecule.

However, the molecular structure and vibrational spectra of the 5-AU molecule was already reported by our group [6]. In this present investigation, frontier molecular orbitals (FMOs) analysis, density of states (DOS) spectral analysis, solvent effect on UV-Visible spectra, first order hyperpolarizability calculations, natural bond orbital (NBO) analysis, molecular electrostatic potential (MEP) surface analysis and local reactivity descriptors calculations of the 5-AU molecule are reported. In addition, the molecular docking analysis was also performed for the title molecule against four targeted proteins such as hCA I, hCA II, hCA IX and hCA XII.

2 Computational details

2.1 Quantum Chemical Calculations

The importance of quantum chemical methods in studying electronic and molecular properties of nucleoside bases such as purine and pyrimidine bases, has been well recognised. The global minimum energy molecular structure was optimized by the DFT/B3LYP method with cc-pVTZ basis set using Gaussian 09 program [21]. The molecular structure, frontier molecular orbitals (FMOs) and molecular electrostatic potential (MEP) surface were visualized by the GaussView 05 [22] visualizing program. The FMOs, first order hyperpolarizability and NBO calculations were carried out for the optimized structure of the molecule by the DFT/B3LYP method with cc-pVTZ basis set. The Gauss-Sum 3.0 program [23] was used to simulate the density of states (DOS) spectrum. The solvent effect on UV–Visible spectrum of the molecule was studied by the time dependent-density functional theory (TD-DFT)/B3LYP method associated with the polarizable continuum model (PCM) using cc-pVTZ basis set for various solvents such as water, ethanol, methanol, acetone and DMSO. In the PCM model, all the solvents were treated as a continuum dielectric medium and the 5-AU molecule was considered as a solute in a cavity surrounded by solvents. The NBO calculations were carried out using NBO 3.1 program as implemented in the Gaussian 09 program [21]. Mulliken atomic charge and local reactivity descriptors values were calculated using Mulliken population analysis by performing the single point energy calculation of N, (N – 1) and (N + 1) species of the molecule with 6-31G (d, p) basis set. All the DFT calculations were done at the ground state energy level of the 5-AU molecule without applying any constraint on the potential energy surface.

2.2 Molecular Docking

Molecular docking studies explore the possible binding mode of the title compound to its target protein. Its process involves the prediction of ligand orientation into its targeted binding site [24]. The molecular docking analysis was performed using AutoDock Tools-1.5.4 interfaced with the MGL Tools-1.5.4 package [25] and the ligand-protein binding pose was visualized by PyMOL molecular graphics system (version 1.7.4.5 Edu) [26]. The title molecule (5-AU) was used as a ligand and the four targeted proteins hCA I (PDB ID: 2FW4), hCA II (PDB ID: 2HNC), hCA IX (PDB ID: 3IAI) and hCA XII (PDB ID: 4HT2) were selected for the present docking analysis. The ligand PDB file was generated by using the optimized molecular structure of the 5-AU molecule. The three-dimensional (3D) coordinates of the targeted proteins were downloaded from the Research Collaboratory for Structural Bioinformatics (RCSB) protein data bank [27], with a resolution of 2.5 Å. The targeted proteins were prepared by the following steps (i) the AutoDockTools graphical user interface [25] was used to remove the ligand and water molecules present in

the targeted proteins and (ii) then polar hydrogen and Kollman charges were added in the targeted proteins. The AutoGrid 4.2 [28] was used to create affinity grid centered on the active site with grid size 120×120×120 with a spacing of 1.0 Å. The rigid targeted protein and flexible ligand docking were performed by using AutoDock 4.2 with the Lamarckian genetic algorithm applying the following protocol: trials of 100 dockings, energy evaluations of 25,000,000, population size of 200, a mutation rate of 0.02, a crossover rate of 0.8, and an elitism value of 1. The docking results were analyzed by comparing the binding energy values obtained by docking confirmations.

3 Results and Discussion

3.1 Frontier molecular orbitals (*FMOs*) *analysis*

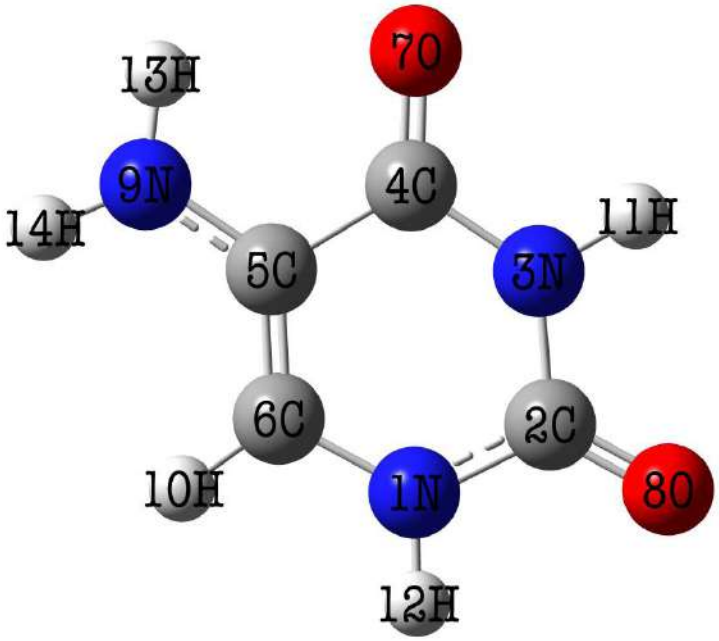

Fig. 1. The optimized molecular structure of 5-aminouracil.

The optimized molecular structure of 5-AU is shown in Fig 1. The highest occupied molecular orbital (HOMO) and lowest unoccupied molecular orbital (LUMO) are known as FMOs, which are used to determine the way in which a molecule interacts with other species. The HOMO energy characterizes the ability of electron giving and LUMO energy characterizes the ability of electron accepting [29]. The FMOs plays an important role in the electric and optical properties in addition to UV–Vis spectra and quantum chemistry [30]. The HOMO–LUMO gap helps in explaining the kinetic stability and the chemical reactivity of the molecule, which are important parameters in analyzing its electronic properties. A molecule with a small HOMO–LUMO gap is usually related with a low kinetic stability, high chemical reactivity and is also called as soft molecule [31]. The FMOs of the molecule are shown in Fig 2(a) and the FMOs related molecular properties were calculated using Koopman's theorem [32], which are listed in Table 1. As shown in Fig 2(a), the positive phase is represented in red color and the negative phase is represented in green color. The calculated low energy gap value (4.45 eV) confirms that the 5-AU molecule has higher chemical reactivity and explains the intramolecular charge transfer interaction within the molecule, which influences its biological activity [32]. The energy needed to remove an electron from the filled orbital is known as ionization energy (I), $I = -E_{HOMO}$ and the energy released when an electron is added to an unfilled orbital

is termed as electron affinity (A), $A = -E_{LUMO}$. The calculated high ionization energy value (5.86 eV) and low electron affinity value (1.41 eV) of the molecule reveal the possibility of electrophilic and nucleophilic attack, respectively [33]. The global hardness, $\eta = ½ (E_{LUMO} - E_{HOMO})$; global softness, $S = 1/\eta$; electronic chemical potential, $\mu = ½ (E_{LUMO} + E_{HOMO})$; and global electrophilicity index, $\omega = \mu^2/2\eta$ of the molecule were also calculated. The calculated higher hardness (2.23 eV) and lower softness (0.45 eV) values indicate the stability of the molecule. The low chemical potential value (–3.64 eV) and electrophilicity index value (2.97 eV) of the molecule also confirm the chemical stability of the molecule, which is comparable with the potential bioactive molecules [32] .

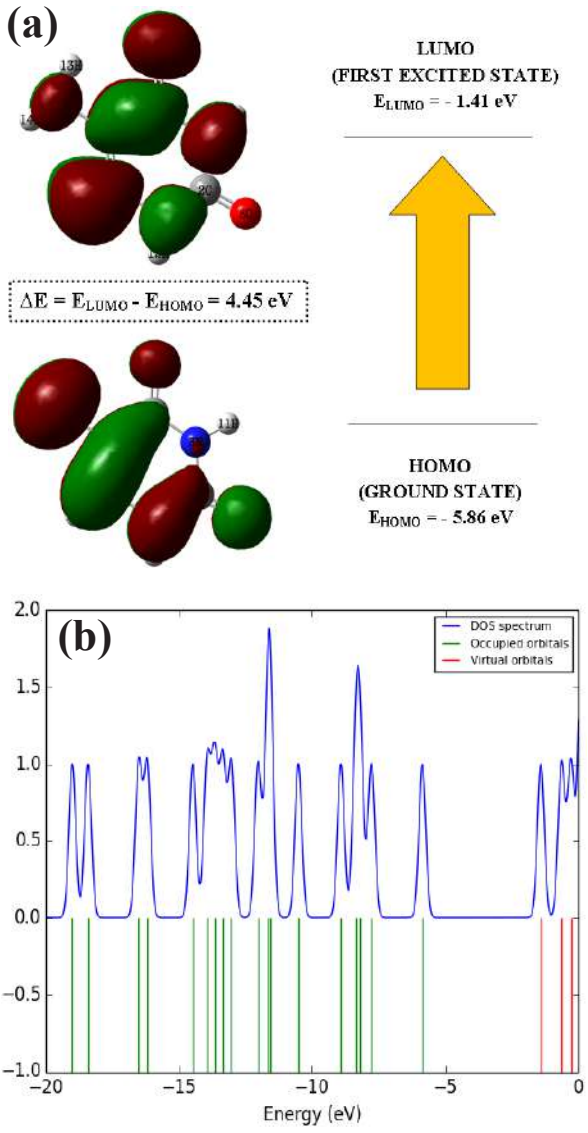

Fig 2. The (a) frontier molecular orbitals and (b) density of states spectrum of the 5-aminouracil molecule.

The density of states (DOS) spectrum of the 5-AU molecule was simulated using Gauss-sum 2.2 program [23] and shown in Fig 2(b). The DOS spectrum is used to calculate the group contributions to

the molecular orbitals (HOMO and LUMO) which show the visual representation of occupied orbitals, virtual orbitals, HOMO, LUMO energy levels and the energy band gap of the molecule [34]. Hence the DOS spectrum was simulated by convoluting the molecular orbital information with Gaussian curves of unit height [35]. These results further validated the FMOs analysis. The green and blue lines in the DOS spectrum represent the occupied and virtual orbitals, respectively.

Table 1. The calculated FMOs related molecular properties of the 5-aminouracil molecule

Molecular properties	Energy (eV)
E_{HOMO}	– 5.86
E_{LUMO}	– 1.41
Energy gap	4.45
Ionization energy (I)	5.86
Electron Affinity (A)	1.41
Global hardness (η)	2.23
Global Softness (S)	0.45
Chemical potential (μ)	–3.64
Electrophilicity index (ω)	2.97

3.2 Solvent effect on the UV-Visible spectrum

The solvent effect on UV-Visible spectra and the corresponding electronic transitions of the molecule were predicted using TD-DFT/B3LYP method with cc-pVTZ basis set. The TD-DFT calculation is a powerful tool for investigating the static and dynamic properties of the molecules in their excited states [35]. The simulated UV-Visible spectra of 5-AU molecule for gas phase and various solvents such as water, methanol, ethanol, acetone and DMSO are shown in Fig 3. The calculated absorption wavelength (λ), excitation energies (E) and oscillator strength (f) for gas phase and varies solvents are listed in Table 2. As shown in Fig 3, the first peak was observed as most intense around 228 nm and 236 nm for gas and solvents, respectively. The second peak was observed around 305 nm and 314 nm in gas phase and solvents, respectively. The observed peaks in the region 200 - 400 nm indicate that the molecule is colorless and the electronic property of the molecule is independent of the solvents. Moreover, the corresponding information could be retrieved through the higher oscillator strength and absorptivities in solvents than in gas phase. Thus solvent eases the absorption with the maximum oscillator strength in DMSO. In addition, an impressive bathochromic shift and a hyperchromic shift were observed in the UV-vis absorption peaks when the molecule goes from the gas phase to solvent phase, which is due to the dipole-dipole interaction between solvent and solute molecule [35].

Table 2. The calculated absorption wavelength λ (nm), excitation energy values E (eV), oscillator strength (f) and orbital contributions for 5-aminouracil molecule with its assignments.

Solvents	λ (nm)	E (eV)	f	Orbital Contributions	Assignments
Gas	227.71	5.4448	0.2018	H→L+3 (96%)	π→ π*
	305.13	4.0633	0.1174	H→L (97%)	n→ π*
Water	236.68	5.2385	0.2715	H-1→L (23%), H→L+4 (70%)	π→ π*
	314.14	3.9468	0.1420	H→L (98%)	n→ π*
Methanol	236.78	5.2094	0.0233	H→L+4 (81%), H-1→L (6%), H→L+2 (8%)	π→ π*
	313.95	3.9492	0.1418	H→L (98%)	n→ π*

Ethanol	236.83	5.2352	0.0154	H→L+4 (87%), H-1→L (4%), H→L+2 (5%)	π→ π*
	314.20	3.9460	0.1442	H→L (98%)	n→ π*
Acetone	236.84	5.2349	0.0758	H→L+2 (26%) H→L+4 (68%)	π→ π*
	314.11	3.9472	0.1441	H→L (98%)	n→ π*
DMSO	237.56	5.2191	0.0009	H→L+2 (97%)	π→ π*
	314.89	3.9374	0.1478	H→L (98%)	n→ π*

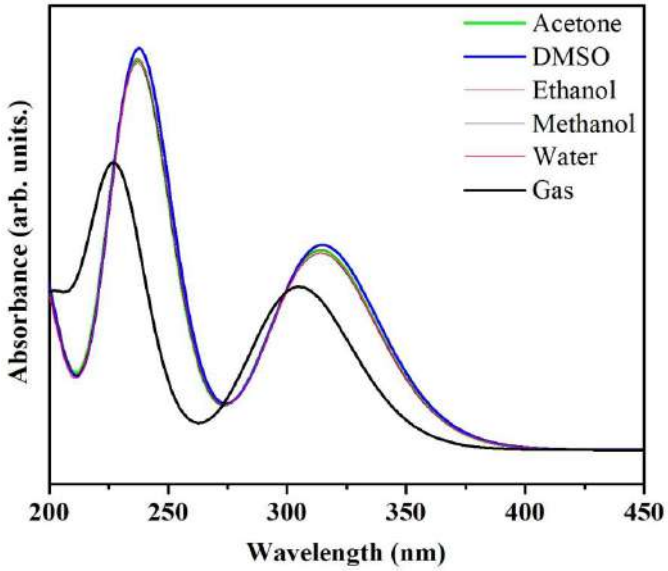

Fig 3. The simulated UV-Visible spectra of 5-aminouracil molecule in gas phase and various solvents.

3.3 First order hyperpolarizability

Nonlinear optical effects arise from the interactions of electromagnetic fields in various media to produce new fields altered in phase, frequency, amplitude or other propagation characteristics from the incident fields [36]. The NLO response materials are providing the key functions for frequency shifting, optical switching, optical modulation, and optical logic for the developing technologies in areas such as communication, signal processing and optical interconnections [32]. The electric dipole moment (μ), polarizability (α) and first order hyperpolarizability (β) of the 5-AU molecule were calculated based on the finite field approach. In the presence of an applied electric field, the energy of a system is a function of the electric field. The first order hyperpolarizability is a third rank tensor, which can be described by a 3×3×3 matrix. The 27 components of the 3D matrix can be reduced to 10 components because of the Kleinman symmetry [37]. The components of β are defined as the coefficients in the Taylor series expansion of the energy in the external electric field. When the external electric field is weak and homogeneous, the Taylor series expansion becomes

$$E = E^0 - \mu_\alpha F_\alpha - 1/2\alpha_{\alpha\beta}F_\alpha F_\beta - 1/6\beta_{\alpha\beta\gamma}F_\alpha F_\beta F_\gamma + ...$$

where E^0 is the energy of the unperturbed molecules, F_α is the field at the origin, μ_α, $\alpha_{\alpha\beta}$ and $\beta_{\alpha\beta\gamma}$ are the components of the dipole moment, polarizability and first order hyperpolarizability, respectively.

The total static dipole moment μ, the mean polarizability α_0, the anisotropy of the polarizability Δα and the mean first order hyperpolarizability β using the *x*, y and *z* components are defined as:

Dipole moment is

$$\mu = \left(\mu_x^2 + \mu_y^2 + \mu_z^2\right)^{1/2}$$

Static polarizability is

$$\alpha_0 = \frac{\alpha_{xx} + \alpha_{yy} + \alpha_{zz}}{3}$$

the anisotropy of the polarizability ($\Delta\alpha$) is

$$\Delta\alpha = 2^{-1/2}\left[(\alpha_{xx} - \alpha_{yy})^2 + (\alpha_{yy} - \alpha_{zz})^2 + (\alpha_{zz} - \alpha_{xx})^2 + 6\alpha_{xz}^2\right]^{1/2}$$

First order hyperpolarizability is

$$\beta = \left(\beta_x^2 + \beta_y^2 + \beta_z^2\right)^{1/2}$$

where

$$\beta_x = (\beta_{xxx} + \beta_{xyy} + \beta_{xzz})$$

$$\beta_y = (\beta_{yyy} + \beta_{xxy} + \beta_{yzz})$$

$$\beta_z = (\beta_{zzz} + \beta_{xxz} + \beta_{yyz})$$

$$\beta = [(\beta_{xxx} + \beta_{xyy} + \beta_{xzz})^2 + (\beta_{yyy} + \beta_{xxy} + \beta_{yzz})^2 + (\beta_{zzz} + \beta_{xxz} + \beta_{yyz})^2]^{1/2}$$

The calculated dipole moment (μ), polarizability (α) and first order hyperpolarizability (β) values of the 5-AU molecule are listed in Table 3. The mean polarizability α_0 and the anisotropy of the polarizability ($\Delta\alpha$) of 5-AU molecule were calculated as 11.577 $\times 10^{-24}$ esu and 8.576 $\times 10^{-24}$ esu, respectively. The total dipole moment and the first order hyperpolarizability values of the molecule were obtained as 4.8961 Debye and 1.685 $\times 10^{-30}$ esu, respectively. Hence the total dipole moment is approximately three times greater than that of urea and first order hyper polarizability is approximately five times greater than that of urea. The calculated dipole moment and first order hyperpolarizability values of urea were obtained as 1.5348 Debye and 0.3328 $\times$ 10^{-30} esu, respectively using B3LYP method with cc-pVTZ basis set. These results are comparable with the reported values of uracil derivatives [38,39]. Table 3 shows that the highest value of first order hyperpolarizability is obtained in the direction of β_{xxx}, and subsequently delocalization of electron cloud is more in that direction. In addition, the calculated high β value of the molecule reveals that the electrons transfer from donor orbitals to acceptor orbitals, which is responsible for the NLO properties of the molecule. Hence, the title molecule can be used for NLO applications.

Table 3. The electric dipole moment, polarizabilty and first order hyper polarizabilty of the 5-aminouracil molecule.

Dipole moment (μ)		Polarizabilty (α)		First order hyperpolarizabilty (β)	
Parameter	Value (DB)	Parameter	esu ($\times 10^{-24}$)	Parameter	esu ($\times 10^{-33}$)
μ_x	–2.2061	α_{xx}	16.197	β_{xxx}	997.685
μ_y	–4.3709	α_{xy}	-0.904	β_{xxy}	298.387
μ_z	0.0030	α_{yy}	12.186	β_{xyy}	802.161
μ	**4.8961**	α_{xz}	0.000	β_{yyy}	877.489
		α_{yz}	-0.000	β_{xxz}	0.408
		α_{zz}	6.349	β_{xyz}	0.077
		α_0	**11.577**	β_{yyz}	0.383
		$\Delta\alpha$	**8.576**	β_{xzz}	–02.095
				β_{yzz}	–234.042
				β_{zzz}	0.443
				β	1685.456
				β = **1.685$\times 10^{-30}$ esu**	

3.4 Natural bond orbital analysis

Hydrogen bonding, intra- and inter- molecular charge transfer interactions taking place in the molecule can be analyzed using natural bond orbital (NBO) analysis [40]. NBO analysis was performed using NBO 3.1 program [41], which is implemented in Gaussian 09 software, based on DFT/B3LYP method with cc-pVTZ basis set. The stabilization energy E(2) associated with the delocalization of each donor (i) to acceptor (j) was calculated on the basis of second-order Fock matrix perturbation theory and listed in Table 4. The stabilization interaction energy of the orbitals is directly proportional to the energy difference between the interacting orbitals of the effective donors and acceptors, which accounts for the intramolecular charge transfer (ICT) and hydrogen bond formation in the molecule. The higher stabilization energy value was obtained for the interaction between LP of N1 and π * (C2-O8) orbital, which confirms the ICT in the molecule. Table 4 shows that the higher stabilization also mainly arises from the LP of N3 to π* (C4-O7), LP of N3 to π* (C2-O8), LP of N9 to π* (C5-C6) and LP of N1 to π* (C5-C6) transitions, which are responsible for the ICT of the title molecule. The stabilization interaction between the LP orbitals and anti-bonding π orbitals is a common molecular feature of the pharmaceutical compounds [29]. Hence, the obtained results confirm that the significant ICT from LP orbitals to anti-bonding π orbitals takes place within the molecule which causes the molecule to be more reactive and bioactive.

Table 4. Second order perturbation theory analysis of Fock matrix of 5-aminouracil molecule by NBO analysis.

Donor(i)	ED (i) (e)	Acceptor (j)	ED (j) (e)	E(2)[a] (Kcal/mol)	E (j) −E (i)[b] (arb. units)	F(i,j)[c] (arb. units)
σ (N1 - C6)	1.9852	σ* (C2 - O8)	0.0097	2.55	1.43	0.05
σ (N1 - C6)	1.9852	σ* (C5 - N9)	0.0137	3.75	1.29	0.06
σ (N1 - H12)	1.9855	σ* (C2 - N3)	0.0842	3.23	1.09	0.05
σ (N1 - H12)	1.9855	σ* (C5 - C6)	0.0173	2.20	1.29	0.05
σ (C2 - N3)	1.9864	σ* (C4 - O7)	0.0093	2.00	1.43	0.05
π (C2 - O8)	1.9929	π* (C2 - O8)	0.3895	2.50	0.38	0.03
σ (N3 - C4)	1.9890	σ* (C2 - O8)	0.0097	2.00	1.44	0.05
σ (N3 - H11)	1.9846	σ* (N1 - C2)	0.0781	3.05	1.10	0.05
σ (N3 - H11)	1.9846	σ* (C4 - C5)	0.0669	2.74	1.10	0.05
σ (C4 - C5)	1.9679	σ* (N3 - H11)	0.0136	2.62	1.06	0.05
σ (C4 - C5)	1.9679	σ* (C5 - C6)	0.0173	2.77	1.28	0.05
σ (C4 - C5)	1.9679	σ* (C6 - H10)	0.0123	3.08	1.08	0.05
σ (C4 - C5)	1.9679	σ* (N9 - H14)	0.0068	2.97	1.11	0.05
π (C4 - O7)	1.9835	π* (C5 - C6)	0.2906	4.90	0.40	0.04
σ (C5 - C6)	1.9784	σ* (N1 - H12)	0.0118	2.00	1.15	0.04
σ (C5 - C6)	1.9784	σ* (C4 - C5)	0.0669	2.09	1.20	0.05
σ (C5 - C6)	1.9784	σ* (C5 - N9)	0.0137	2.87	1.22	0.05
π (C5 - C6)	1.8541	π* (C4 - O7)	0.3321	19.13	0.30	0.07
σ (C5 - N9)	1.9890	σ* (C5 - C6)	0.0173	3.32	1.43	0.06
σ (C6 - H10)	1.9799	σ* (N1 - C2)	0.0781	3.78	0.99	0.06
σ (C6 - H10)	1.9799	σ* (C4 - C5)	0.0669	4.11	0.99	0.06
σ (N9 - H13)	1.9895	σ* (C5 - C6)	0.0173	4.54	1.26	0.07
σ (N9 - H14)	1.9908	σ* (C4 - C5)	0.0669	3.04	1.11	0.05

LP (1) N1	1.6637	π* (C2 - O8)	0.3895	58.13	0.28	0.12
LP (1) N1	1.6637	π* (C5 - C6)	0.2906	34.22	0.30	0.09
LP (1) N3	1.6466	π* (C2 - O8)	0.3895	53.81	0.28	0.11
LP (1) N3	1.6466	π* (C4 - O7)	0.3221	54.43	0.28	0.11
LP (1) O7	1.9799	σ* (C4 - C5)	0.0669	2.04	1.13	0.04
LP (2) O7	1.8622	σ* (N3 - C4)	0.0789	26.42	0.68	0.12
LP (2) O7	1.8622	σ* (C4 - C5)	0.0669	18.07	0.70	0.10
LP (2) O8	1.8414	σ* (N1 - C2)	0.0781	24.81	0.68	0.12
LP (2) O8	1.8414	σ* (C2 - N3)	0.0842	26.02	0.65	0.12
LP (1) N9	1.8180	π* (C5 - C6)	0.2906	43.47	0.27	0.10

[a] Stabilisation (delocalisation) energy.
[b] Energy difference between i (donor) and j (acceptor) NBO orbitals.
[c] Fock matrix element i and j NBO orbitals.

3.5 MEP surface

The total electron density mapped with MEP surface analysis provides a visual representation of the chemically active sites of a molecule and also enhances the understanding of molecular reactivity, electrophilic reactions, substituent effects, intra and intermolecular interactions [32]. Figure 4 shows the MEP surface of the 5-AU molecule. The red, yellow, light blue and blue color in the MEP surface specify the electron rich, slightly electron rich, slightly electron deficient and electron deficient regions, respectively. The region around the oxygen atoms was found to be electron rich (red), which is due to the lone pair of oxygen atom. The electron deficient (blue) region of the molecule was surrounded over the hydrogen atoms H11, H12, H13 and H14 and only the hydrogen atom H10 was found to be slightly electron deficient (light blue), which is due to the electronegative nitrogen atoms being attached with the hydrogen atoms H11, H12, H13 and H14. The neutral electrostatic potential (green) envelopes over the π-system of the uracil ring. The electrophilic region of the molecule was predicted around the hydrogen atoms of the molecule and uracil ring. MEP analysis indicates that the hydrogen atoms (H11, H12, H13 and H14) and urcail ring oxygen atoms (O8 and O7) are possible sites for the electrophilic and nucleophilic attacks, respectively [42].

3.6 Mulliken atomic charge distribution and Local reactivity descriptors analysis

The Mulliken atomic charge distribution of a molecule has significant influence on its dipole moment, polarizability, electronic structure, vibrational modes, and model of electrostatic potential outside the molecular surface, which also describes the process of electronegativity equalization of the molecule [43]. The calculated anion, neutral and cation Mulliken atomic charge distribution values of the molecule are listed in Table 5. From the Table 5, it is clear that the uracil ring carbon atom C2 of the molecule has higher positive charge value, which is because the carbon atom C2 was attached with the electronegative atoms N1, N3 and O8 [35]. The amino group nitrogen atom N9 of the molecule has higher positive value, which is because the nitrogen atom N9 was attached with electropositive atoms C5, H13 and H14. The Mulliken atomic charge distribution of the molecule shows that all the hydrogen and carbon atoms have positive charge values. The hydrogen atoms H11, H12, H13 and H14 possess higher positive charge value than the hydrogen atom H10, which is because the electronegative nitrogen atoms (N1, N3 and N9) are attached with those hydrogen atoms. The higher negative charge values were predicted for the electronegative atoms N1, N3, N9, O7 and O8 of the molecule. Further, the Mulliken atomic charge distribution analysis confirms that the hydrogen atoms (H11, H12, H13 and H14) and electronegative atoms (N9, N3, N1, O7 and O8) are more possible sites for the electrophilic and nucleophilic attack, respectively [42].

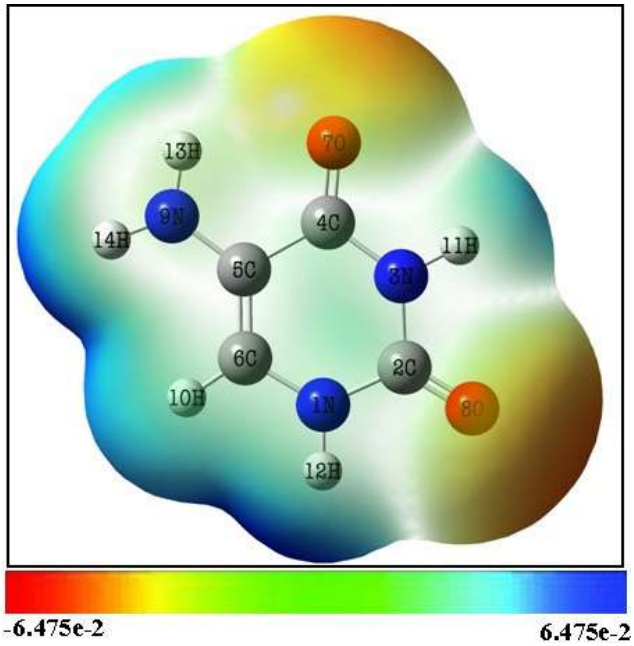

Fig 4. The molecular electrostatic potential surface of the 5-aminouracil molecule.

Table 5. The calculated Mulliken atomic charge distribution of the 5-aminouracil molecule.

Atom	Mulliken atomic charge values		
	Neutral q (N)	Cation q(N–1)	Anion q (N+1)
N1	–0.486	–0.401	–0.561
C2	0.580	0.579	0.968
N3	–0.558	–0.524	–0.553
C4	0.275	0.267	0.927
C5	0.060	0.135	2.593
C6	0.287	0.344	–0.882
O7	–0.520	–0.412	–0.577
O8	–0.512	0.354	–0.586
N9	–0.641	–0.430	–0.733
H10	0.156	0.225	–1.680
H11	0.355	0.398	0.362
H12	0.348	0.403	–0.336
H13	0.347	0.398	0.242
H14	0.310	0.373	–0.185

The local reactivity descriptors such as Fukui functions, local softness and local electrophilicity indices are useful in predicting the possible reactive sites of the particular molecule, which play an important role in drug designing [19]. In this work, the local reactivity descriptors such as Fukui functions f_k^+, f_k^-, f_k^0, local softness s_k^+, s_k^-, s_k^0 and local electrophilicity indices ω_k^+, ω_k^-, ω_k^0

are calculated for the 5-AU molecule using Mulliken population analysis to predict the possible electrophilic and nucleophilic reactive sites of the molecule [44]. The calculated local reactivity descriptors of the 5-AU molecule are listed in Table 6.

Fukui function defines the more reactive regions in the molecule, which lead to the selectivity towards specific chemical events in a molecule [45]. The higher Fukui function f_k^+ values for nucleophilic attack were predicted as in the order of C5 > C4 > C2 > N3 > H11 atoms. These are possible sites for the nucleophilic attack. The higher Fukui function f_k^- values for electrophilic attack were predicted as in the order of C4>C2>N3> H11>H13 atoms and these are the possible sites for electrophilic attacks. The higher Fukui function values for radical attack were predicted for the molecule as in the order of C5>C4> C2> N3>H11atoms. These results are further validated by local softness and electrophilicity values [46]. Since, the individual Fukui functions are basis set and correlation effect dependent, the relative electrophilicity $(f_k^+)/(f_k^-)$ and relative nucleophilicity $(f_k^-)/(f_k^+)$ values were determined [47] and listed in Table 6. The site having the high relative nucleophilicity is the most probable site to be attacked by an electrophile, and the site with high relative electrophilicity is the most probable site to be attacked by a nucleophile. Hence the results further confirm that the uracil ring carbon atom C2 is possible site to be attacked by a nucleophile and amino group nitrogen atom N9 is possible site to be attacked by a electrophile.

Table 6. The local reactivity descriptors of 5-aminouracil molecule.

Atom	Fukui functions			Local softness			Local electrophilicity indices			Relative electrophi-licity	Relative nucleo-philicity
	(f_k^+)	(f_k^-)	(f_k^0)	(s_k^+)	(s_k^-)	(s_k^0)	(ω_k^+)	(ω_k^-)	(ω_k^0)	$(f_k^+)/(f_k^-)$	$(f_k^-)/(f_k^+)$
N1	–0.075	–0.085	–0.160	–0.034	–0.038	–0.072	–0.223	–0.253	0.475	0.882	1.133
C2	0.388	0.001	0.389	0.175	0.000	0.175	1.152	0.003	1.155	388.000	0.003
N3	0.005	-0.034	–0.029	0.002	-0.015	-0.013	0.015	–0.101	–0.086	-0.147	–6.800
C4	0.652	0.008	0.660	0.293	0.004	0.297	1.936	0.024	1.960	81.500	0.012
C5	2.533	-0.075	2.458	1.140	-0.034	1.106	7.523	-0.223	7.300	–33.773	–0.029
C6	–1.169	-0.057	–1.226	-0.526	-0.026	-0.552	-3.472	-0.169	-3.641	20.509	0.049
O7	–0.057	-0.108	–0.165	-0.026	-0.049	-0.074	-0.169	-0.321	-0.490	0.528	1.894
O8	–0.074	-0.158	–0.232	-0.033	-0.071	-0.104	-0.219	-0.469	-0.689	0.468	2.135
N9	–0.092	-0.211	–.303	-0.041	-0.095	-0.136	-0.273	-0.627	-0.899	0.436	2.293
H10	–1.836	-0.069	–1.905	-0.826	-0.031	-0.857	-5.453	-0.205	-5.658	26.609	0.038
H11	0.007	-0.043	–0.036	0.003	-0.019	-0.016	0.021	-0.128	-0.107	–0.162	–6.143
H12	–0.684	-0.055	–0.739	-0.308	-0.025	-0.333	-2.032	-0.163	-2.195	12.436	0.080
H13	–0.105	-0.051	–0.156	-0.047	-0.023	-0.070	-0.313	-0.152	-0.463	2.059	0.486
H14	–0.495	-0.063	–0.558	-0.223	-0.028	-0.251	-1.470	-0.187	-1.657	7.857	0.127

3.7 Molecular docking analysis

Molecular docking has become an increasingly important tool for drug discovery. The molecular docking approach can be used to model the interaction between a small molecule and a protein at the atomic level, which allows us to characterize the behaviour of small molecules in the binding site of target proteins as well as to elucidate fundamental biochemical processes [48]. In this work, the molecular docking analysis was carried out for flexible ligand (5-AU) and the rigid targeted proteins including hCA I, hCA II, hCA IX and hCA XII. The ligand molecule was docked well with all the targeted proteins. The lowest energy docked

poses of the ligand with various targeted proteins are shown in Figure 5, which shows the preferred binding orientation of the ligand molecule. The dotted yellow lines show the hydrogen bond formation between the ligand and targeted proteins. The length of the hydrogen bonds between the ligand and the amino acid residues in the targeted proteins were also shown in Fig 5.The docking parameters for the first three ranks (1, 2 and 3) such as binding energy, inhibition constant and intermolecular energy of the ligand with the targeted proteins are listed in Table 7.

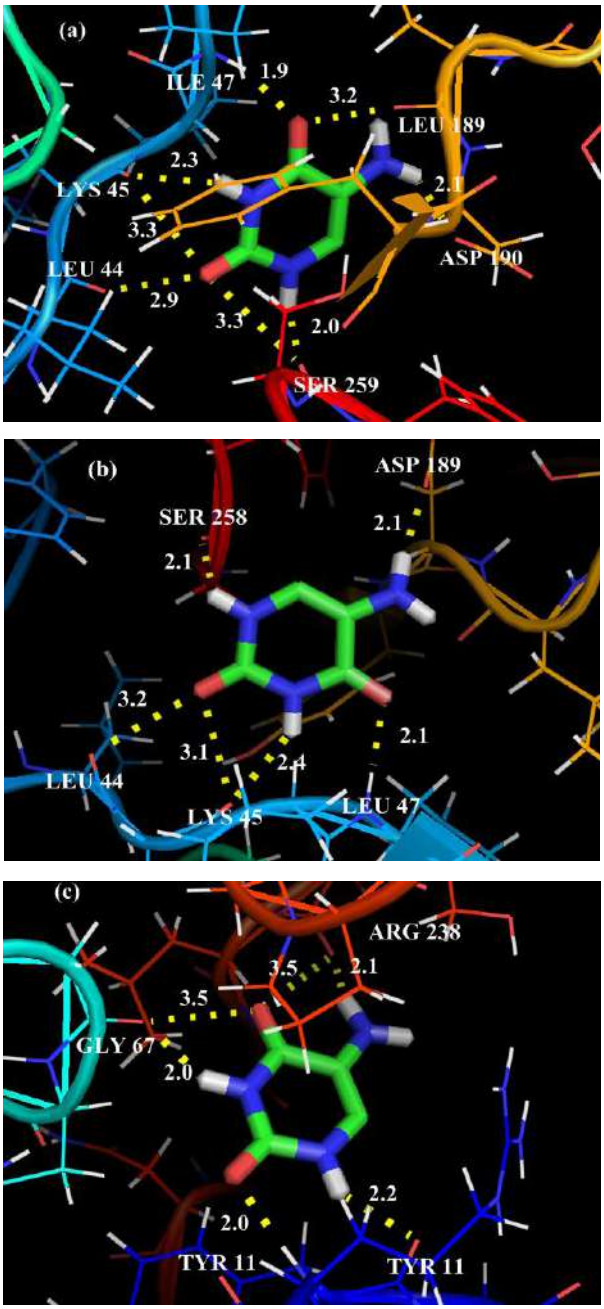

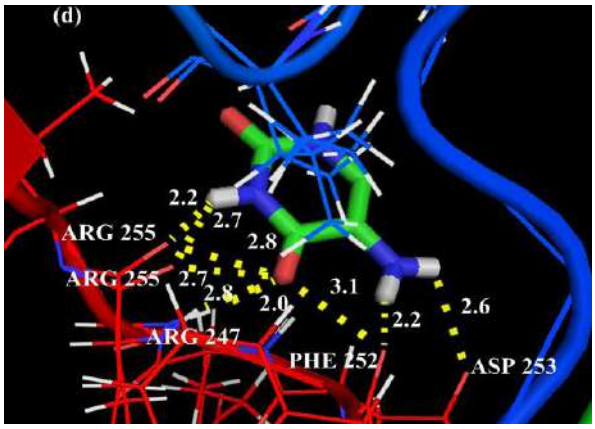

Fig 5. Lowest energy docked poses of the 5-aminouracil (5-AU) ligand with various targeted proteins such as (a) hCA I, (b) hCA II, (c) hCA IX and (d) hCA XII.

Table 7. The obtained docking parameters of the 5-aminouracil molecule on their rank calculated by Autodock

Ligand	Target protein (receptor)	Docking Parameters based on the rank								
		Binding energy (Kcal/mol)			Inhibition constant (mM)			Intermolecular energy (Kcal/mol)		
		1	2	3	1	2	3	1	2	3
5-AU	hCA I	–4.39	–4.02	–3.89	0.61	1.12	1.41	–4.69	–4.32	–4.19
	hCA II	–4.10	–3.96	–3.78	0.98	1.25	1.69	–4.40	–4.26	–4.08
	hCA IX	–4.09	–3.66	–3.44	0.99	2.07	3.02	–4.39	–3.96	–3.74
	hCA XII	–3.82	–3.74	–3.71	1.57	1.83	1.90	–4.12	–4.03	–4.01

These results indicate that the ligand (5-AU) exhibits the lower binding energy and inhibition constant for the targeted protein hCA I. The formation of more hydrogen bonds leads to the decreasing hydrophilicity and increasing hydrophobicity, which stabilizes the 5AU–hCA I complex system. The 3D representation of docked ligand (5-AU) at the binding site (hydrophobic pocket) of the targeted protein hCA I and 2D representation of the interactions of ligand (5-AU) with the targeted protein are shown in Fig 6(a) and (b), respectively. As shown in Fig 6(a) and (b), the uracil ring oxygen atom O7 forms the hydrogen bond with the amino acid residues ILE 47 and LEU 189, the uracil ring oxygen atom O8 forms the hydrogen bond with the amino acid residues LEU 44, LYS 45 and SER 259, the uracil ring hydrogen atoms 11H and 12H form hydrogen bonds with the amino acid residues LYS 45 and SER 259, respectively and the amino group hydrogen atom 14H forms hydrogen bond with the amino acid residue ASP 190. Generally, the formation of hydrogen bonds decreases the hydrophilicity and increases the hydrophobicity in the ligand-protein complex, which confirms the high affinity between the 5AU-hCA I complex system. The uracil ring oxygen O7 is located inside the hydrophobic pocket (Fig 6(a)), which has been formed by the residues ILE 47 and LEU 189 and involved in the hydrophobic interaction with uracil oxygen atom O7. Figure 6(b) clearly shows that the uracil ring interacts with the residues ILE 47 and LEU 189 through π-π and van der Walls interactions, respectively. These findings confirm that the ligand (5-AU) molecule can act as a potential inhibitor against hCA I, which regulates the high intraocular pressure (IOP) [13]. The regulation of IOP can treat the glaucoma. Ramachandran plot of targeted protein hCA I with binding amino acid ILE 47 in yellow is shown in Fig 6(c). Ramachandran plot is mainly useful because it defines the residues in regions that are energetically more favorable and unfavorable, for drug designing [49]. On observing the Ramachandran plot, the energetically allowed regions of the binding amino acid residue ILE 47 has the torsion angle psi (ψ) of –74.66 against phi

(φ) of –124.29 which lies in the most allowed blue region of the plot as seen in Fig 6(c). Hence, the obtained results confirm that the title molecule has the inhibition nature against the hCA I enzyme, which will pave the way for developing the effective therapies in the treatment of glaucoma.

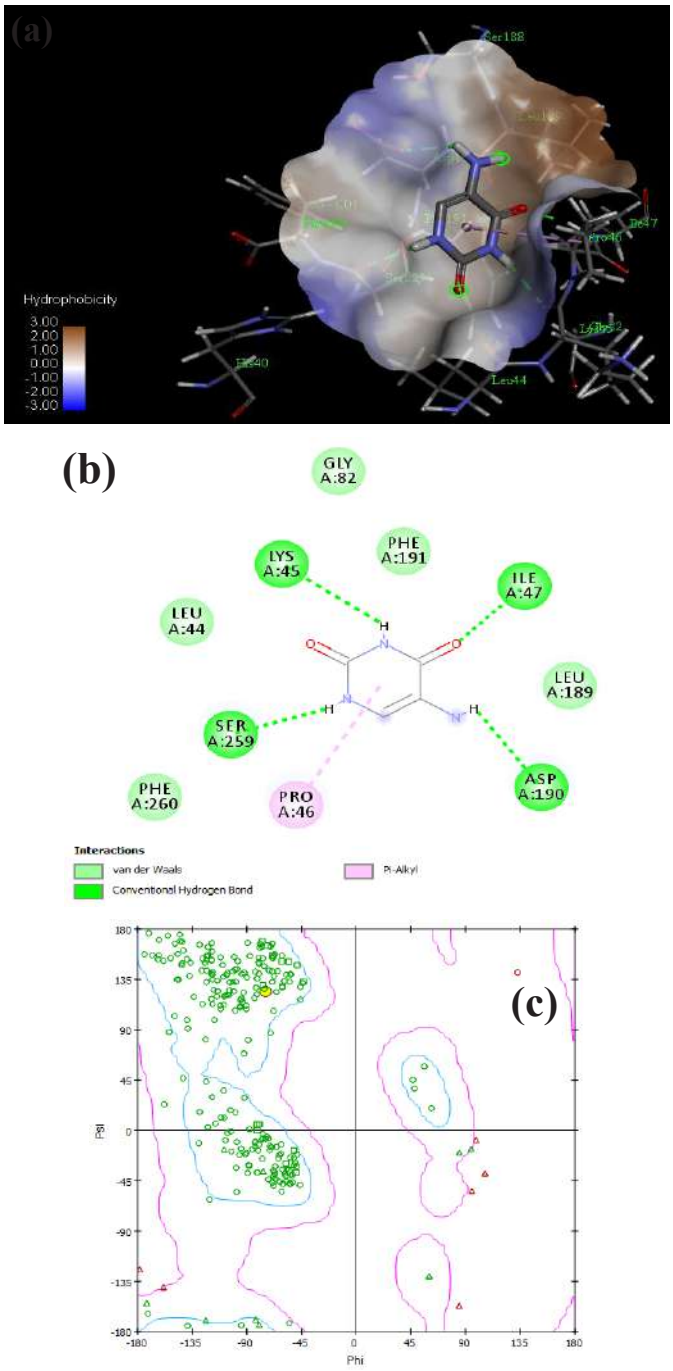

Fig 6. (a) The 3D representation of docked ligand (5-AU) at the binding site (hydrophobic pocket) of the targeted protein hCA I, (b) 2D representation and (c) Ramachandran plot of targeted protein hCA I with binding amino acid ILE 47 (yellow).

4 Conclusion

The quantum chemical and molecular docking studies of 5-AU molecule were performed. FMOs analysis shows that the title molecule has low energy gap value which evidences the ICT interaction in the molecule. The FMOs results were validated using the density of states spectrum. The calculated first order hyperpolarizability value reveals the NLO property of the molecule. The solvent effect on UV-Visible spectra and the corresponding electronic transitions of the molecule were predicted. The MEP surface and local reactivity descriptors analyses confirm the possible sites for the electrophilic and nucleophilic attack in the molecule. The natural bond orbital analysis also predicts the bioactivity of the molecule. The molecular docking studies conclude that the title molecule has strong binding affinity towards the targeted protein hCA I than other targeted proteins. Hence, these results pave the way for developing the effective therapies in the treatment of glaucom**a**.

Acknowledgements

The author (R. Premkumar) thanks the College Management for encouragement and permission to carry out this work and also thank the P.G. and Research Department of Physics, N. M. S. S. V. N. College, Nagamalai, Madurai-19, for providing the Gaussian 09 program package.

References

1. Mohamed M S, Awad S M, Sayed A I, *Molecules*, 15(2010)1882-1890.
2. Yagi K, Akimoto K, Mimori N, Miyake T, Kudo M, Arai K, Ishii S, *Pest Manage Sci*, 56(2000)65-73.
3. Isobe Y, Tobe M, Inoue Y, Isobe M, Tsuchiya M, Hayashi H, *Bioorg Med Chem*, 11(2003)4933-4940.
4. Presant C A, Wolf W, Waluch V, Wiseman C, Kennedy P, Blayney D, Brechner R R, *Lancet*, 343(1994)1184-1187.
5. Palafox M A, Nielsen O F, Lang K, Garg P, Rastogi V K, *Asian Chem Lett*, 8(2004)81-93.
6. Palafox M A, Tardajos G, Martı´nez G G-, Rastogi V K, Mishra D, Ojha S P, Kiefer W, *Chem Phys*, 340(2007)17-31.
7. Fathalla O A, *Arch Pharmacol Res*, 22(1999)571-574.
8. Ulvenlund S, Georgopoulou A S, Mingos D M P, Baxter I, Lawrence S E, White A J P, Williams D J, *J Chem Soc Dalton Trans*, 11(1998)1869-1878.
9. Hueso-Ureña F, Illán-Cabeza N A, Moreno-Carretero M N, Martínez-Martos J M, Ramírez-Expósito M J, *J Inorg Biochem*, 94(2003)326-334.
10. Güney M, Çavdar H, Şentürk M, Ekinci D, *Bioorg Med Chem Lett*, 25(2015)3261-3263.
11. Alper Turkoglu E, Senturk M, Supuran C T, Ekinci D, *J Enzyme Inhib Med Chem*, 32(2017)74-77.
12. Li F R, Fan Z F, Qi S J, Wang Y S, Wang J, Liu Y, Cheng M S, *Molecules*, 22(2017)785; doi.org/10.3390/molecules22050785.
13. Supuran C T, *Nat Rev Drug Discov*, 7(2008)168-181.
14. Balaydin H T, Durdağı S, Ekinci D, Şentürk M, Göksu S, Menzek A, *J Enzyme Inhib Med Chem*, 27(2012)467-475.
15. Supuran C T, *Bioorg Med Chem Lett*, 20(2010)3467-3474.
16. Waheed A, Sly W S, *Gene*, 623(2017)33-40.
17. Djeradi H, Rahmouni A, Cheriti A, *J Mol Model*, 20(2014)2476.
18. Lienard P, Gavartin J, Boccardi G, Meunier M, *Pharm Res*, 32(2015)300-310.
19. Asath R M, Premkumar R, Mathavan T, Benial A M F, *Spectrochim Acta,* A 175(2017)51-60.
20. Sroka Z, Żbikowska B, Hładyszowski J, *J Mol Model*, 21(2015)307.
21. Frisch M J, Trucks G W, Schlegel H B, Scuseria G E, Robb M A, Cheeseman J R, Scalmani G, Barone V, Mennucci

B, Petersson G A, Nakatsuji H, Caricato M, Li X, Hratchian H P, Izmaylov A F, Bloino J, Zheng G, Sonnenberg J L, Hada M, Ehara M, Toyota K, Fukuda R, Hasegawa J, Ishida M, Nakajima T, Honda Y, Kitao O, Nakai H, Vreven T, Montgomery J A, Jr., Peralta J E, Ogliaro F, Bearpark M, Heyd J J, Brothers E, Kudin K N, Staroverov V N, Kobayashi R, Normand J, Raghavachari K, Rendell A, Burant J C, Iyengar S S, Tomasi J, Cossi M, Rega N, Millam J M, Klene M, Knox J E, Cross J B, Bakken V, Adamo C, Jaramillo J, Gomperts R, Stratmann R E, Yazyev O, Austin A J, Cammi R, Pomelli C, Ochterski J W, Martin R L, Morokuma K, Zakrzewski V G, Voth G A, Salvador P, Dannenberg J J, Dapprich S, Daniels A D, Farkas O, Foresman J B, Ortiz J V, Cioslowski J, Fox D J, Gaussian 09, Revision C. 02, Gaussian Inc., Wallingford CT, (2009).

22. Ray Dennington, Todd Keith, John Milam, Gauss View, Version 5, Semichem Inc., Shawnee Mission KS, (2009).
23. O'boyle N M, Tenderholt A L, Langner K M, *J Comput Chem*, 29(2008)839-845.
24. Kitchen D B, Decornez H, Furr J R, Bajorath J, *Nat Rev Drug Discov,* 3(2004)935-949.
25. Morris G M, Goodsell D S, Halliday R S, Huey R, Hart W E, Belew R K, Olson A J, J *Comput Chem*, 19(1998)1639-1662.
26. The PyMOL Molecular Graphics System, Version 1.7.4.5 Schrödinger, LLC.
27. http://www.rcsb.org/pdb.
28. Morris G M, Goodsell D S, Halliday R S, Huey R, Hart W E, Belew R K, Olson A J, *J Comput Chem*, 10(1996)293-304.
29. Premkumar S, Rekha T N, Asath R M, Mathavan T, Benial A M F, *Eur J Pharm Sci*, 82(2016)115-125.
30. Babu B, Chandrasekaran J, Mohanbabu B, Matsushita Y, Saravanakumar M, *RSC Adv*, 6(2016)110884-110897.
31. Narayan V, Mishra H N, Prasad O, Sinha L, *Comput Theor Chem*, 973(2011)20-27.
32. Asath R M, Premkumar R, Mathavan T, Benial A M F, *J Mol Struct*, 1143(2017)415-423.
33. Wilson A M M, Mitnik D G, *J Mol Struct* (*Theochem*), 716(2005)67–72.
34. Gumus P, Tamer O, Avci D, Atalay Y, *Indian J Phys*, 90(2016)79-89.
35. Saravanan S, Blachandran V, *Spectrochim Acta,* A 130(2014)604-620.
36. Rajamani T, Muthu S, Karabacak M, *Spectrochim Acta,* A 108(2013)186-196.
37. Kleinman D A, *Phys Rev*, 126(1962)1977-1979.
38. Pir H, Günay N, Tamer O, Avci D, Atalay Y, *Spectrochim Acta,* A 112(2013)331-342.
39. Gümüs H P, Tamer O, Avci D, Tarcan E, Atalay Y, *J Phys Chem*, *A* 88(2014)2348-2358.
40. Weinhold F, Landis C R, Valency and Bonding: A Natural Bond Orbital Donor-Acceptor Perspective, (Cambridge University Press, New York), 2005.
41. Glendening E D, Reed A E, Carpenter J E, Weinhold F, NBO Version 3.1, TCI, University of Wisconsin, Madison, 1998.
42. Yesilkaynak T, Binzet G, Emen F M, Florke U, Kulcu N, Arslan H, *Eur J Chem*, 1(2010)1-5.
43. Šponer J, Leszczynski J, Hobza P, *Biopolymers*, 61(2002)3-31.
44. Fukui K, Theory of Orientation and Stereoselection. Springer–Verlag, Berlin, 1975.
45. Abbaz T, Bendjeddou A, Didier Villemin D, *Pharmaceutical & Biological Evaluations*, 5(2018); doi: 10.26510/2394-0859.pbe.2018.04
46. Chattaraj P K, Maiti B, Sarkar U, *J Phys Chem A*, 107(2003)4973-4975.
47. Karthick T, Tandon P, *J Mol Model*, 22(2016)142; doi: 10.1007/s00894-016-3015-z
48. Meng X Y, Zhang H X, Mezei M, Cui M, *Curr Comput-Aid Drug*, 7(2011)146-157.
49. Yamamoto A, Tomoo K, Hara T, Murata M, Kitamura K, Ishida T, *J Biochem*, 127(2000)635-643.

[*Received*: 1.3.2019: *revised recd*: 15.3.2019; *accepted*: 29.3.2019]